INTERNATIONAL JOURNAL OF HYDROGEN ENERGY 39 (2014) 7147–7157

Available online at www.sciencedirect.com

ScienceDirect

journal homepage: www.elsevier.com/locate/he

Large-eddy simulation of lean hydrogen–methane turbulent premixed flames in the methane-dominated regime

*Francisco E. Hernández-Pérez**, *Clinton P.T. Groth*, *Ömer L. Gülder*

University of Toronto Institute for Aerospace Studies, 4925 Dufferin Street, Toronto, Ontario M3H 5T6, Canada

ARTICLE INFO

Article history:
Received 18 December 2013
Received in revised form
29 January 2014
Accepted 4 February 2014
Available online 20 March 2014

Keywords:
Turbulent premixed combustion
Large-eddy simulation
Hydrogen–methane mixtures
Presumed conditional moment
Flame prolongation of intrinsic low-dimensional manifold

ABSTRACT

The application of large-eddy simulation (LES) to the prediction of H_2-enriched lean methane–air turbulent premixed combustion is considered. A presumed conditional moment (PCM) subfilter-scale combustion model is coupled with the flame prolongation of intrinsic low-dimensional manifold (FPI) chemistry tabulation technique. The LES and PCM-FPI modelling procedures are then applied to the prediction of laboratory-scale axisymmetric Bunsen-type turbulent premixed flames. Both premixed methane–air and H_2-enriched methane–air flames are considered and the predicted solutions are examined and compared to available experimental data. The enriched flame has 20% H_2 in terms of mole fraction and lies in the methane-dominated regime of hydrogen–methane mixtures. The LES simulations predict similar qualitative trends to those found in the experiments for flame height and curvature. The addition of H_2 decreases the flame height and broadens the curvature probability density functions, which show a Gaussian-type shape centred around zero. Moreover, the enriched flame displays a higher degree of wrinkling with sharper ridges of negative curvature and larger pockets of positive curvature. Overall, the proposed treatment for the PCM-FPI combustion model, in terms of progress variable and tabulated data, seems to perform well for the H_2-enriched methane flame in the methane-dominated regime.

1. Introduction

Despite the widely-recognized potential of H_2 as a cleaner and sustainable source of energy, the approaches for the transition from a fossil-based to hydrogen-based economy are still under discussion and the implementation of the hydrogen-based economy is expected to take decades [1,2]. Muradov and Veziroğlu [2] have extensively reviewed such transition, highlighting carbon-neutral technologies and processes (see, e.g., Ref. [3]).

H_2 and hydrocarbon fuel blends appear to be a promising option to synergistically pave the way toward pure hydrogen-based combustion systems while alleviating green-house gas and pollutant emissions related to fossil fuel combustion. The possibility of using hydrogen-enriched hydrocarbon fuels as a

* *Corresponding author*. Current address: Combustion Technology Research Group, Eindhoven University of Technology, Eindhoven, Netherlands. Tel.: +31 40 247 5995; fax: +31 40 243 3445.
E-mail address: F.E.Hernandez.Perez@tue.nl (F.E. Hernández-Pérez).
http://dx.doi.org/10.1016/j.ijhydene.2014.02.028

means for enabling greater stability of lean premixed flames with significantly reduced emissions of nitrogen oxides is also very appealing.

While promising, the wide-spread application of hydrogen-enriched hydrocarbon fuels in practical premixed combustion devices has been limited by an incomplete understanding of hydrogen-enriched combustion. In particular, the current understanding, in terms of theoretical and computational models, is unable to fully explain the experimental observations for such flames.

A number of previous studies have been conducted on the performance and emission characteristics of practical devices using H_2-enriched hydrocarbon fuels [4–7]. It has been found that hydrogen enrichment extends the lean stability limit and decreases emissions of carbon monoxide (CO), nitrogen oxides (NO_x), and unburned hydrocarbons (UHC) in spark-ignition engines, power-generation gas turbines, and aircraft gas turbines. There have also been several studies focused on fundamental aspects of hydrogen–hydrocarbon flames. It has been reported that H_2-enriched flames display higher laminar flame speeds, extended lean flammability limits, and augmented resistance to strain [8–12]. Moreover, experiments in swirl-stabilized burners [13,14] have been conducted to investigate the stabilization and blowout characteristics of H_2-enriched methane–air premixed flames. It has also been shown that the addition of H_2 to methane (CH_4) extends the flame lean stability limit, allowing stable burner operation at lower flame temperatures and reducing NO_x emissions. Of particular note to the present work, Di Sarli and Di Benedetto [15] have identified three regimes of laminar burning velocity in terms of the mole fraction of H_2 in the fuel, $\varkappa(\varkappa = n_{H_2}/(n_{H_2} + n_{CH_4}))$. They are: (i) the methane-dominated combustion regime $(0 < \varkappa < 0.5)$; (ii) the transition regime $(0.5 \leq \varkappa \leq 0.9)$; and (iii) the methane-inhibited hydrogen combustion regime $(0.9 < \varkappa < 1)$. Numerical treatment for the so-called "methane-dominated regime" is the primary focus here.

There have been only a few previous computational studies of multi-dimensional H_2-enriched methane–air turbulent premixed flames. Hawkes and Chen [16] performed two-dimensional (2D) direct numerical simulations (DNS) of freely propagating flames in decaying turbulence with complex reduced chemistry (15-step reaction mechanism). Dunstan and Jenkins [17] simulated 2D premixed kernels in decaying turbulence using DNS with detailed chemistry. Day et al. [18] performed a 2D study to characterize lean methane–air flames with significant hydrogen addition, including detailed transport and chemical kinetics. Finally, Vreman et al. [19] carried out three-dimensional DNS of slot Bunsen flames with tabulated chemistry. In all the DNS simulations cited above, complex chemistry and preferential diffusion were taken into account and their relevance to characterize the flame behaviour were recognized.

This study considers the application of large-eddy simulation (LES) and appropriate subfilter-scale (SFS) modelling to the prediction of H_2-enriched lean methane–air turbulent premixed combustion. In particular, a presumed conditional moment (PCM) SFS combustion model [20] is coupled with the flame prolongation of intrinsic low-dimensional manifold (FPI) chemistry tabulation technique [21]. The LES and PCM-FPI modelling procedures are then applied to the prediction of laboratory-scale axisymmetric Bunsen-type turbulent premixed flames. Both premixed methane–air and H_2-enriched methane–air flames are considered and the predicted solutions are examined and compared to measured data from the experimental study of Halter et al. [22]. The enriched flame has 20% H_2 by volume and lies in the methane-dominated regime as defined by Di Sarli and Di Benedetto [15]. The turbulence intensity for both flames was relatively low and they are expected to correspond to the classical flamelet regime. The capability of the LES model to predict the observed behaviour is examined for this range of turbulent reactive flows.

2. Large-eddy simulation of turbulent premixed flames

The LES framework developed by Hernández-Pérez et al. [23,24] is used for performing this study. The framework is now briefly summarized, along with the PCM-FPI combustion model.

2.1. Favre-filtered governing equations

For the LES computations considered here, the Favre-filtered form of the Navier–Stokes equations governing compressible flows of a thermally perfect reactive gaseous mixture of N species, neglecting Dufour, Soret and radiation effects, is used to describe the turbulent premixed combustion processes. Relevant flow parameters, φ, are either filtered using a low-pass spatial filtering procedure or Favre-filtered using a mass-weighted filter to yield $\overline{\varphi}$ or $\tilde{\varphi}$, respectively. The resulting equations are given by

$$\frac{\partial(\overline{\rho})}{\partial t} + \frac{\partial(\overline{\rho}\tilde{u}_i)}{\partial x_i} = 0, \tag{1}$$

$$\frac{\partial(\overline{\rho}\tilde{u}_i)}{\partial t} + \frac{\partial}{\partial x_j}\left(\overline{\rho}\tilde{u}_i\tilde{u}_j + \delta_{ij}\overline{p} - \check{\tau}_{ij}\right) = \overline{\rho}g_i + A_1, \tag{2}$$

$$\frac{\partial(\overline{\rho}\tilde{E})}{\partial t} + \frac{\partial}{\partial x_i}\left[\left(\overline{\rho}\tilde{E} + \overline{p}\right)\tilde{u}_i + \dot{q}_i\right] - \frac{\partial}{\partial x_j}\left(\check{\tau}_{ij}\tilde{u}_i\right) = \overline{\rho}g_i\tilde{u}_i + B_1 + B_2 + B_3, \tag{3}$$

$$\frac{\partial(\overline{\rho}\tilde{Y}_k)}{\partial t} + \frac{\partial(\overline{\rho}\tilde{Y}_k\tilde{u}_i)}{\partial x_i} + \frac{\partial\mathcal{J}_{k,i}}{\partial x_i} = \overline{\dot{\omega}}_k + C_1, \tag{4}$$

where $\overline{\rho}$ is the filtered mixture density, $\tilde{u}_i$ is the Favre-filtered mixture velocity, $\overline{p}$ is the filtered mixture pressure, $\tilde{Y}_k$ is the Favre-filtered mass fraction of species k, $\tilde{E}$ is the Favre-filtered total mixture energy (including chemical energy) given by $\tilde{E} = \sum_{k=1}^{N}\tilde{Y}_k(\check{h}_k + \Delta h^0_{f,k}) - \overline{p}/\overline{\rho} + \widetilde{u_i u_i}/2$; $\check{h}_k$, $\Delta h^0_{f,k}$ and $\overline{\dot{\omega}}_k$ are the sensible enthalpy (evaluated in terms of the Favre-filtered temperature), heat of formation and the filtered reaction rate of species k, respectively, and g_i is the acceleration due to gravity. The filtered equation of state adopts the form $\overline{p} = \overline{\rho}R\tilde{T}$, assuming that the SFS temperature-species correlation is negligible. Here, $\tilde{T}$ is the Favre-filtered mixture temperature and R is the gas constant. The resolved stress tensor, $\check{\tau}_{ij}$, the

resolved total heat flux, $\check{q}_i$, and the resolved species diffusive fluxes, $\check{\mathcal{J}}_{k,i}$, are evaluated in terms of the filtered quantities.

The terms, A_1, B_1, B_2, B_3, and C_1, arise from the low-pass filtering process and require modelling. These terms are expressed as

$$A_1 = -\frac{\partial\left[\overline{\rho}\left(\widetilde{u_i u_j} - \tilde{u}_i\tilde{u}_j\right)\right]}{\partial x_j},\quad B_1 = -\frac{\partial\left[\overline{\rho}\left(\widetilde{hu_i} - \check{h}\tilde{u}_i\right)\right]}{\partial x_i},$$

$$B_2 = -\frac{1}{2}\frac{\partial\left[\overline{\rho}\left(\widetilde{u_j u_j u_i} - \tilde{u}_j\tilde{u}_j\tilde{u}_i\right)\right]}{\partial x_i},\quad C_1 = -\frac{\partial\left[\overline{\rho}\left(\widetilde{Y_k u_i} - \tilde{Y}_k\tilde{u}_i\right)\right]}{\partial x_i},$$

$$B_3 = -\frac{\partial\left[\sum_{k=1}^{N}\Delta h^0_{f,k}\overline{\rho}\left(\widetilde{Y_k u_i} - \tilde{Y}_k\tilde{u}_i\right)\right]}{\partial x_i},$$

and must be modelled for closure of the filtered equation set. The subfilter stresses, $\sigma_{ij} = -\overline{\rho}(\widetilde{u_i u_j} - \tilde{u}_i\tilde{u}_j)$, are modelled using an eddy-viscosity type model with $\sigma_{ij} = 2\overline{\rho}\nu_t(\check{S}_{ij} - \delta_{ij}\check{S}_{ll}/3) + \delta_{ij}\sigma_{ll}/3$. The SFS turbulent viscosity, ν_t, is prescribed herein by using a one-equation model [25] for the SFS turbulent kinetic energy, k_Δ. Standard gradient-based approximations are used in this work for the modelling of the SFS fluxes B_1, B_3, and C_1. The subfilter turbulent diffusion term, B_2, is modelled as suggested by Knight et al. [26] with $-\overline{\rho}(\widetilde{u_i u_i u_j} - \tilde{u}_i\tilde{u}_i\tilde{u}_j)/2 = \sigma_{ij}\tilde{u}_i$. In the expressions above, Einstein summation convention applies to the indices i, j and l.

2.2. PCM-FPI combustion model

A primary challenge in the development of LES for turbulent reactive flows is the accurate and reliable modelling of the interaction between turbulence and chemistry and the specification of the filtered reaction rates, $\overline{\dot{\omega}}_k$. For LES of turbulent premixed combustion, this is further complicated by the large number of species and complexity of the chemical kinetic mechanisms for typical hydrocarbon fuels and the fact that the chemical reactions occur in a thin reacting layer at extremely small scales that are not resolvable on typical LES grids. This places particular importance on the SFS modelling of these terms.

The PCM-FPI [20] is an approach that combines a presumed probability density function (PDF) approach with FPI tabulated chemistry based on prototypical flames with simplified flow geometry [21]. The FPI tabulation technique, which is very similar to the flamelet-generated manifold (FGM) technique [27–29], helps to greatly reduce the costs of performing reactive flow computations involving large chemical kinetic mechanisms and the use of a presumed PDF allows for the economical treatment of the effects of subfilter turbulence on the filtered reaction rates.

For the premixed flames of interest here, steady one-dimensional laminar premixed flamelets are used in the construction of the FPI tabulated chemistry. Relevant chemical parameters, ϕ_j, such as species mass fractions and/or reaction rates, are related to a single progress of reaction variable, Y_c. For a given equivalence ratio, φ_0, the relationship for $\varphi_j = \varphi_j^{\mathrm{FPI}}(\phi_0, Y_c)$ and the progress variable is established by a mapping of computed solutions for steady-state one-dimensional laminar premixed flames expressed as a function of position normal to the flame front on to the Y_c-space. For LES of turbulent premixed flames, filtered quantities are then obtained via

$$\tilde{\varphi}_j = \int_0^1 \varphi_j^{\mathrm{FPI}}(c^*)\tilde{P}(c^*)\,\mathrm{d}c^*, \tag{5}$$

where c is the progress variable and $\tilde{P}(c^*)$ is the filtered probability density function of c, which needs to be specified.

The PDF of c is taken here to be a β-distribution [30,31] and can be constructed from the resolved or filtered progress variable, $\tilde{c}$, and its SFS variance, $c_v = \widetilde{cc} - \tilde{c}\tilde{c}$. These two variables, $\tilde{c}$ and c_v, are directly linked to the progress of reaction $\tilde{Y}_c$ and its SFS variance, Y_{c_v}. The filtered progress variable is defined as the filtered progress of reaction normalized by its value at equilibrium: $\tilde{c} = \tilde{Y}_c/Y_c^{\mathrm{Eq}}(\phi_0)$. The variance of c may be obtained from the variance of the progress of reaction, $Y_{c_v} = \widetilde{Y_c Y_c} - \tilde{Y}_c\tilde{Y}_c$ and expressed as $c_v = Y_{c_v}/Y_c^{\mathrm{Eq}^2}(\phi_0)$.

Note that other choices for the presumed PDF of c are possible, including the original and modified laminar-flame-based PDFs of Bray et al. [32] and Jin et al. [33], respectively. While the correctness of the modified laminar-flame-based PDF of Jin et al. [33] as compared to the β-distribution for premixed flames has been demonstrated by Salehi et al. [34,35], for LES of premixed flames in the flamelet regime with relatively low turbulence intensities, the differences in the predicted solutions obtained using the modified laminar-flame-based and β PDFs have been found to be rather small [34–36]. For this reason, it is felt that the β-PDF is sufficiently accurate for the hydrogen-enriched flames of interest and is used here.

Modelled balance equations are used to determine Y_c and Y_{c_v} [20,30,31]. The modelled transport equation for $\tilde{Y}_c$ has the form

$$\frac{\partial(\overline{\rho}\tilde{Y}_c)}{\partial t} + \frac{\partial(\overline{\rho}\tilde{u}_i\tilde{Y}_c)}{\partial x_i} = \frac{\partial}{\partial x_i}\left[\overline{\rho}\left(\check{\mathcal{D}}_{Y_c} + \mathcal{D}_t\right)\frac{\partial\tilde{Y}_c}{\partial x_i}\right] + \overline{\dot{\omega}}_{Y_c}, \tag{6}$$

where $\overline{\dot{\omega}}_{Y_c}$ is a source term due to chemistry, $\check{\mathcal{D}}_{Y_c}$ is the diffusion coefficient associated with Y_c, and $\mathcal{D}_t$ is the turbulent diffusion coefficient used to model SFS scalar transport. The transport equation for Y_{c_v} is given by

$$\begin{aligned}\frac{\partial(\overline{\rho}Y_{c_v})}{\partial t} + \frac{\partial(\overline{\rho}\tilde{u}_i Y_{c_v})}{\partial x_i} = {}& \frac{\partial}{\partial x_i}\left[\overline{\rho}\left(\check{\mathcal{D}}_{Y_c} + \mathcal{D}_t\right)\frac{\partial Y_{c_v}}{\partial x_i}\right] \\ & + 2\overline{\rho}\left(\check{\mathcal{D}}_{Y_c} + \mathcal{D}_t\right)\frac{\partial\tilde{Y}_c}{\partial x_i}\frac{\partial\tilde{Y}_c}{\partial x_i} - 2\overline{\rho\mathcal{D}_{Y_c}\frac{\partial Y_c}{\partial x_i}\frac{\partial Y_c}{\partial x_i}} \\ & + 2\left(\overline{Y_c\dot{\omega}_{Y_c}} - \tilde{Y}_c\overline{\dot{\omega}}_{Y_c}\right).\end{aligned} \tag{7}$$

The scalar dissipation rate of Y_c,

$$\overline{\chi}_{Y_c} = 2\overline{\rho\mathcal{D}_{Y_c}\frac{\partial Y_c}{\partial x_i}\frac{\partial Y_c}{\partial x_i}},$$

may be decomposed into resolved and unresolved parts as follows:

$$\overline{\chi}_{Y_c} = 2\overline{\rho}\check{\mathcal{D}}_{Y_c}\frac{\partial\tilde{Y}_c}{\partial x_i}\frac{\partial\tilde{Y}_c}{\partial x_i} + 2\overline{s}_{\chi_{Y_c}}.$$

The SFS component is closed with the combined linear relaxation hypothesis and bimodal limit closure proposed by Domingo et al. [30], which takes into account that Y_c is a reactive scalar and its gradient is influenced by chemistry.

It is important to remark that a reaction rate can be written as $\dot{\omega} = \rho\dot{\omega}^*$, therefore $\overline{\dot{\omega}} = \overline{\rho}\widetilde{\dot{\omega}}^*$ and $\overline{Y_c\dot{\omega}_{Y_c}} = \overline{\rho}\widetilde{Y_c\dot{\omega}^*_{Y_c}}$. The latter is a reaction rate term appearing in the transport equation for Y_{c_v}. The terms $\widetilde{\dot{\omega}}^*_{Y_c}$ and $\widetilde{Y_c\dot{\omega}^*_{Y_c}}$ are included in the tabulated database. By introducing the segregation factor, $S_c = c_v/(\tilde{c}(1-\tilde{c}))$, a look-up table of filtered quantities, $\tilde{\varphi}_j^{PCM}(\phi_0, \tilde{c}, S_c)$, can be pre-generated for use in subsequent computations.

2.3. Parallel finite-volume scheme

The Favre-filtered transport equations for a premixed reactive gaseous mixture given by Eqs. (1)–(4) above, along with transport equations for the filtered progress of reaction variable and its variance (Eqs. (6) and (7)) as well as the SFS turbulent kinetic energy, are all solved on multi-block body-fitted meshes consisting of hexahedral cells by employing a second-order accurate parallel finite-volume scheme [23,24,37–42]. The inviscid flux at each cell face is evaluated using limited linear reconstruction [43] and Riemann-solver based flux functions [44,45], while the viscous flux is evaluated utilizing a hybrid average gradient-diamond path method [46]. A standard, explicit, two-stage, second-order-accurate, Runge-Kutta, time-marching scheme is used to integrate forward in time the non-linear, coupled-system of ordinary differential equations resulting from the finite-volume spatial discretization procedure. Parallel implementation of the solution method has been carried out via domain decomposition using the C++ programming language and the MPI (message passing interface) library [47,48]. Second-order accuracy of the finite-volume scheme for discretizations on multi-block body-fitted meshes has been demonstrated in other previous studies [37–40].

3. Tabulated chemistry for H_2-enriched methane–air flames

Previous studies by Fiorina et al. [49] and Galpin et al. [31] have shown that for FPI tabulated chemistry of methane–air combustion based on steady laminar premixed flamelets, an appropriate choice for the progress of reaction variable is $Y_c = Y_{CO_2} + Y_{CO}$. It has also been shown by these authors that it can be sufficient to tabulate the flamelet data for a rather reduced number of species based on their contributions to mixture mass and energy. In fact, just 10 species: CH_4, O_2, N_2, H_2O, CO_2, CO, H_2, H, OH and C_2H_2, are needed to accurately represent the mass and energy of methane–air reactive mixtures [31]. However, in order to improve the prediction of the H_2 mass fraction and allow for the prediction of NO in H_2-enriched methane–air flames, a revised progress of reaction variable is needed and an enlarged set of species must be tracked. Furthermore, to aid in the treatment of the preferential diffusion of H_2, transport equations for the tracked species are solved directly, along with the equations associated with the progress variable and its variance, using reconstructed filtered reaction rates from the pre-computed FPI look-up tables based on a high Damköler number approximation [30,31].

3.1. Selection of progress variable and reduced set of tracked species

In order to assess the FPI tabulation needs for LES of hydrogen-enriched methane combustion, steady-state, one-dimensional solutions of H_2-enriched methane–air laminar premixed flames were first obtained using the Cantera package [50] with detailed chemistry provided by the GRI-Mech 3.0 chemical kinetics mechanism [51]. GRI-Mech 3.0 has been used previously to obtain good predictions of laminar flame speeds, profiles of major species, NO_x levels, and extinction strain rates in agreement with experimental values [10,52]. The generated solutions were confined to the methane-dominated regime and included different levels of enrichment up to a 40% mole fraction of H_2 in the blended fuel, with increments of 5%. The equivalence ratio was varied from values near the lean-flammability limit up to two.

Careful examination and analysis of the laminar premixed flamelet solutions revealed that a suitable single progress of reaction variable for hydrogen-enriched methane combustion, in the methane-dominated regime, is provided by $Y_c = Y_{CO_2} + Y_{NO}$. It was found that this definition of Y_c increases monotonically and can adequately account for the slow chemistry associated with NO for both lean and stoichiometric H_2-enriched methane–air premixed flamelets. Note that previous studies have shown that NO must be included in the definition of the progress of reaction variable in order to: (i) avoid errors in NO mass fraction that can be introduced when employing a progress variable defined only in terms of major species [53,54]; and (ii) properly account for time scales that differ from those of major species [55,56].

Fig. 1(a) and (b) display the NO mass fraction evolution in the progress variable space (normalized progress of reaction variable) corresponding to the proposed progress of reaction and the progress of reaction variable used previously by Fiorina et al. [49], for lean (φ=0.8) and stoichiometric H_2-enriched methane–air premixed flamelets. Magnified views of the regions where NO is reaching its equilibrium value are also displayed in Fig. 1(c) and (d). The profiles of NO mass fraction corresponding to Y_c based on major species show larger slopes when NO is near its equilibrium value, which are almost vertical. This may lead to errors in the tabulated NO mass fraction. On the other hand, the NO profiles corresponding to the new definition of Y_c show smoother and monotone transitions to the equilibrium values, as can be seen in Fig. 1(c) and (d).

Temperature and representative species mass fractions profiles in Y_c-space, associated with the proposed progress of reaction variable, are also depicted in Fig. 2 for premixed flamelets enriched with H_2 by 20% (on a molar basis) and a range of equivalence ratios that includes fuel-rich conditions. It is apparent from the results shown in the figure that the novel Y_c is suitable for lean and stoichiometric conditions, ensuring a one-to-one correspondence between the representative mass fractions and Y_c. However, for the fuel-rich conditions (see Fig. 2(b) for $\varphi = 1.5$ and Fig. 2(c) for $\varphi = 1.25$ and $\varphi = 1.5$), these desirable properties would no longer hold for the proposed progress of reaction variable. Nevertheless, since the scope of this research work is limited to lean flames, the newly defined Y_c is adopted herein.

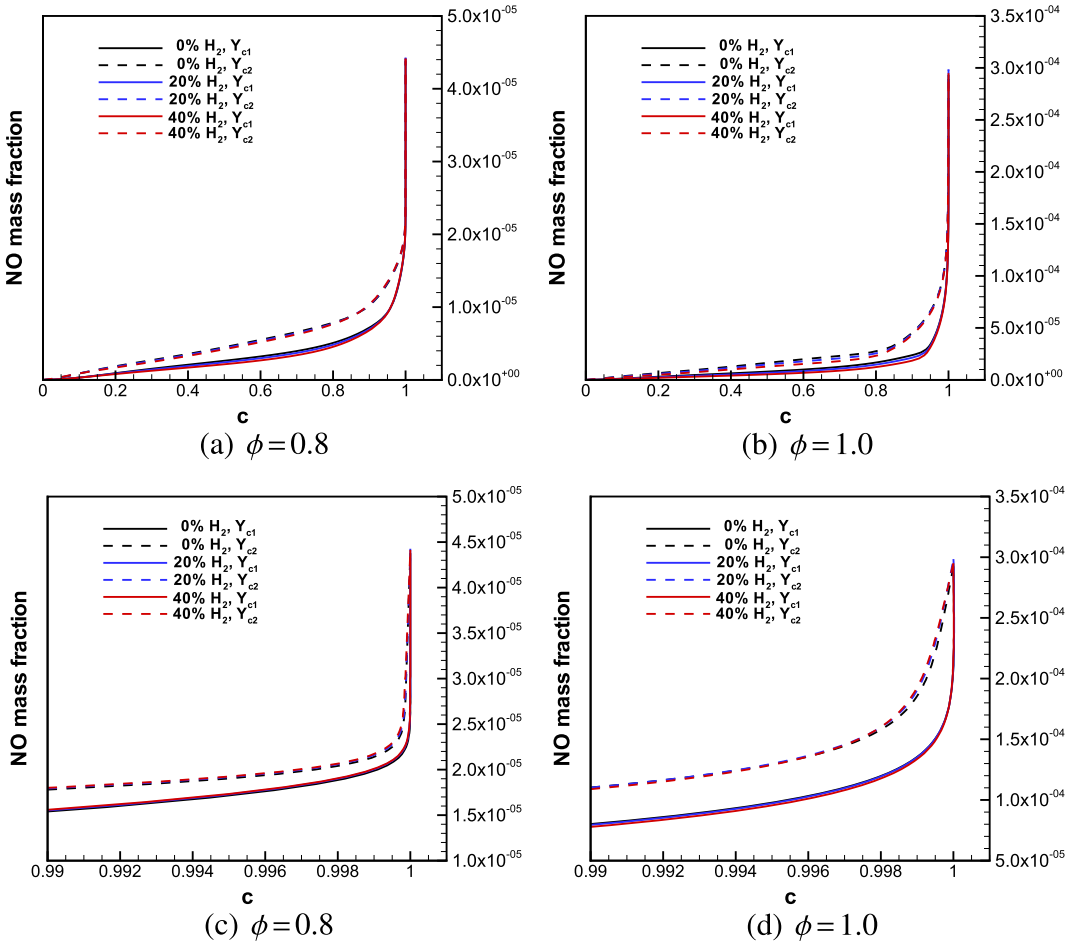

Fig. 1 – NO mass fraction evolution in the progress variable space for $Y_{c1}=Y_{CO_2}+Y_{CO}$ and $Y_{c2}=Y_{CO_2}+Y_{NO}$, corresponding to lean and stoichiometric conditions (ϕ = 0.8 and ϕ = 1.0) with different levels of H_2 (0%, 20%, and 40% on a molar basis) in the blended H_2–CH_4 fuel. One-dimensional steady-state laminar premixed flames. Top: full NO evolution in progress variable space. Bottom: magnified views of the regions where NO is reaching its equilibrium value.

Furthermore, based on contributions to mixture mass, energy, and heat release, the species CH_4, CH_3, O_2, O, N_2, H_2O, CO_2, CO, H_2, H, and OH were selected, in addition to NO. Two further species, C_2H_2 and NH_3, were added to allow for elemental mass balance and absorb inconsistencies for the C and H elements. As a result, the number of species included in the FPI look-up tables for the LES of hydrogen-enriched methane-flames considered here was 14 species.

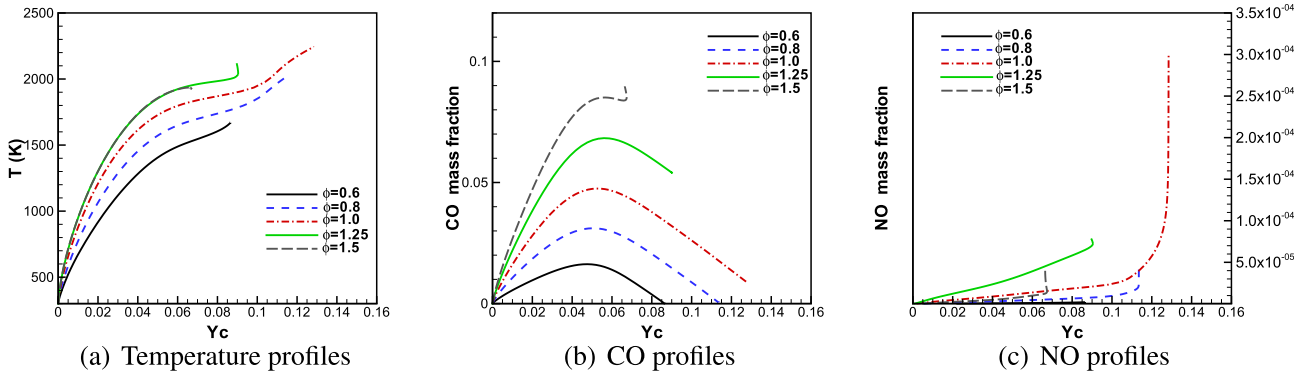

Fig. 2 – Temperature and representative species profiles in the progress of reaction space for $Y_c=Y_{CO_2}+Y_{NO}$, corresponding to lean, stoichiometric, and rich conditions, and 20% H_2 in the blended H_2–CH_4 fuel. One-dimensional steady-state laminar premixed flames.

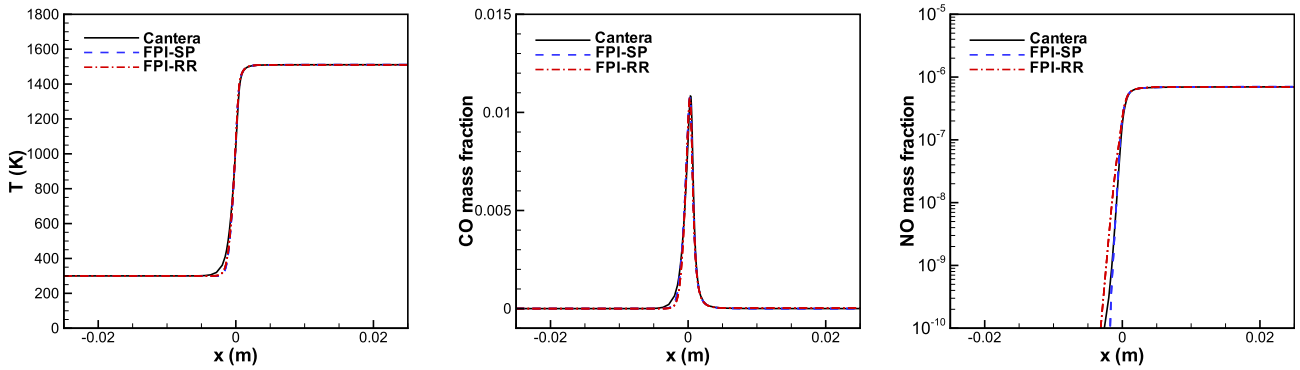

Fig. 3 – Comparison of predicted temperature and CO and NO mass fraction profiles for a one-dimensional premixed laminar CH_4–air flame with $\phi = 0.52$ obtained using the PCM-FPI model with $Y_c = Y_{CO_2} + Y_{NO}$ and 14 species to a detailed chemical kinetic solution obtained using Cantera. FPI-SP: reading mass fractions directly. FPI-RR: transporting the species using reconstructed reaction rates.

3.2. *Performance of proposed tabulation procedure for laminar premixed flames*

The proposed 14-species FPI tabulation method with $Y_c = Y_{CO_2} + Y_{NO}$ was found to yield accurate solutions for steady, one-dimensional, laminar, premixed H_2–CH_4–air flames in the methane-dominated regime to within a few percent of the values of the full chemical kinetic solutions, for thermodynamic properties and major and minor species. For example, consider the comparison of FPI tabulated results obtained using the approach outlined above to detailed chemical kinetic solutions obtained using Cantera given in Figs. 3 and 4 for one-dimensional premixed, laminar methane–air and hydrogen-enriched methane–air (29% H_2 on a molar basis) flames at atmospheric pressure and having a fresh gas temperature of 300 K. The equivalence ratio for both cases is $\varphi = 0.52$. The predicted temperature and CO and NO mass fraction profiles of the one-dimensional flames are displayed in the two figures. Two sets of results for the PCM-FPI approach are given, one based on reading mass fractions directly and the other based on transporting the species with reconstructed reaction rates. The predicted profiles of the species CO and NO closely follow the profiles given by the Cantera solutions. In particular, there is a remarkable agreement for the equilibrium NO levels, which are less than one part per million (ppm) in each case. The PCM-FPI predictions of the laminar flame speed and burned gas temperature for these flames also compare well with those given by Cantera. A summary of flame speed and temperature comparisons are provided in Table 1. Note that the PCM-FPI solutions based on reconstructed reaction rates provide slight improvements in the predictions, particularly for flame temperature.

3.3. *Generation of PCM-FPI tables*

Based on the proposed 14-species set and progress of reaction variable, Y_c, defined by $Y_c = Y_{CO_2} + Y_{NO}$, PCM-FPI look-up tables for hydrogen-enriched methane–air combustion were generated here by using pre-computed laminar premixed flamelet solutions obtained using Cantera and GRI-Mech 3.0.

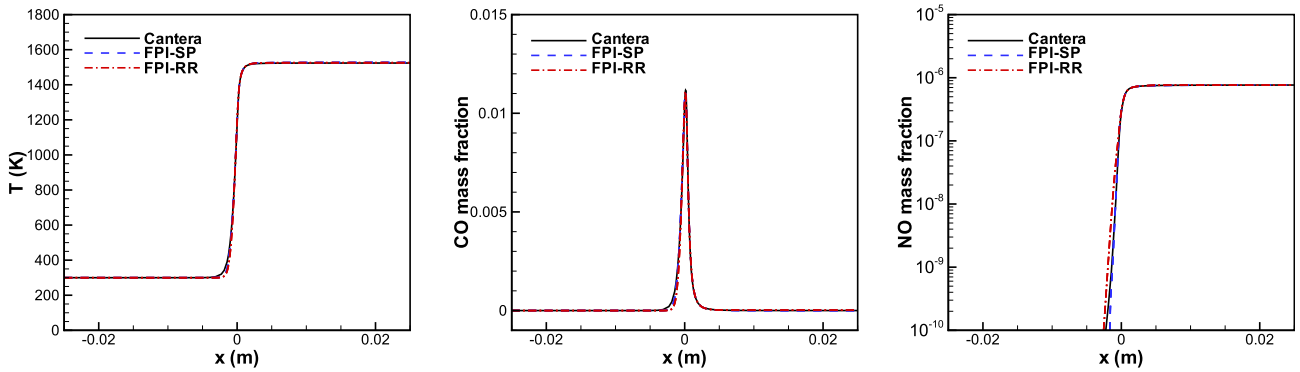

Fig. 4 – Comparison of predicted temperature and CO and NO mass fraction profiles for a one-dimensional premixed laminar H_2–CH_4–air flame (29% H_2 in the fuel) with $\phi = 0.52$ obtained using the PCM-FPI model with $Y_c = Y_{CO_2} + Y_{NO}$ and 14 species to a detailed chemical kinetic solution obtained using Cantera. FPI-SP: reading mass fractions directly. FPI-RR: transporting the species using reconstructed reaction rates.

Table 1 – Summary of predicted flame speeds and temperatures in the burned gas for one-dimensional steady-state CH_4–air ($\varkappa$=0.0) and H_2–CH_4–air ($\varkappa$=0.29) premixed flames at $\phi = 0.52$. PCM-FPI model with 14 species reading mass fractions directly (FPI-SP) and transporting the species using reconstructed reaction rates (FPI-RR).

	Cantera		PCM-FPI			
			FPI-SP		FPI-RR	
$\varkappa$	0.0	0.29	0.0	0.29	0.0	0.29
s_L (m/s)	0.0612	0.0806	0.061	0.081	0.061	0.081
T_b (K)	1510.99	1523.89	1511.02	1526.9	1510.48	1525.9

The flamelet solutions were integrated with β-PDFs for a range of values of both the resolved and SFS variance of the progress variable. Values for the filtered species mass fractions and filtered reaction rates $\widetilde{\dot{\omega}}^*_{Y_c}$ and $\widetilde{Y_c\dot{\omega}}^*_{Y_c}$ were pre-computed and stored for retrieval from the look-up tables, which contained 138 non-uniformly-spaced values of $\tilde{c}$ and 25 non-uniformly-spaced values of S_c.

4. LES results for Bunsen-type premixed flames

LES computations for axisymmetric Bunsen-type turbulent premixed methane–air and H_2-enriched methane–air flames have been performed. The predicted solutions for both flames are examined and further compared to available data from the experiments carried out earlier by Halter et al. [22].

4.1. *Burner setup*

The Bunsen-type flames of interest correspond to lean premixed turbulent conditions at an equivalence ratio of $\varphi = 0.6$ and atmospheric pressure [22]. For the enriched flame, H_2 represents 20% of the blended fuel on a molar basis ($\varkappa = 0.2$). An axisymmetric burner with an inner nozzle diameter of 25 mm was used to generate the premixed turbulent conical flames stabilized by annular pilot flames. The turbulence at the burner exit was characterized by a turbulence intensity $u' = 0.17$ m/s and an integral length scale $L_t = 3$ mm. The mixtures of reactants had a temperature of 300 K and their mean inflow velocity was 2.1 m/s.

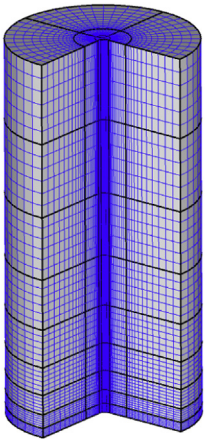

Fig. 5 – Cylindrical computational domain and mesh containing 1,638,400 cells used in the LES predictions of the turbulent premixed Bunsen-type flames.

In the simulations, a cylindrical domain having a diameter of 0.05 m and a height of 0.1 m was employed and discretized with a grid consisting of 1,638,400 hexahedral cells. The cylindrical computational domain and mesh are shown in Fig. 5. The pilot flames were approximated by a uniform inflow of hot combustion products at a velocity of 2.73 m/s. For the burner exit, a uniform mean inflow of reactants with superimposed turbulent fluctuations was prescribed. The same turbulence field was used for both the enriched and pure methane flame simulations. The assumed Schmidt numbers associated with each species, as taken from the Cantera flamelet solutions and used for the Bunsen flame simulations, are given in Table 2.

4.2. *Instantaneous flame fronts*

Three-dimensional views of the predicted instantaneous flame surfaces for both the pure methane and hydrogen-enriched flames, identified by the isotherm $\tilde{T} = 650$ K, are depicted in Fig. 6 corresponding to a physical time t = 56 ms, for which a quasi-steady flame structure has been achieved in each case. The isotherms (light grey) are shown interacting with turbulent structures identified by iso-values of the Q-criterion, $Q = 1606\ s^{-2}$ (cyan). The Q-criterion [57] can be used to visualize the coherent structures of the turbulent velocity field. Positive values of Q are associated with regions where vorticity dominates straining.

From Fig. 6 it is evident that the simulated flames exhibit a wrinkled surface having a similar structure up to 5 cm above the burner exit. Further downstream, the hydrogen enriched

Table 2 – Schmidt numbers of the species for the lean CH_4–air ($\varkappa$=0.0) and H_2–CH_4–air ($\varkappa$=0.2) premixed flames at $\phi = 0.6$, taken from the Cantera solutions in the burned gas.

Schmidt numbers, $\phi = 0.6$							
CH_4–air flame	CH_4	CH_3	O_2	O	CO_2	CO	H_2O
	0.679	0.675	0.749	0.482	0.941	0.751	0.555
	N_2	OH	H_2	H	C_2H_2	NO	NH_3
	0.707	0.491	0.206	0.123	0.887	0.758	0.607
H_2–CH_4–air flame (20% H_2)	CH_4	CH_3	O_2	O	CO_2	CO	H_2O
	0.681	0.677	0.751	0.483	0.941	0.753	0.556
	N_2	OH	H_2	H	C_2H_2	NO	NH_3
	0.712	0.492	0.207	0.124	0.889	0.759	0.608

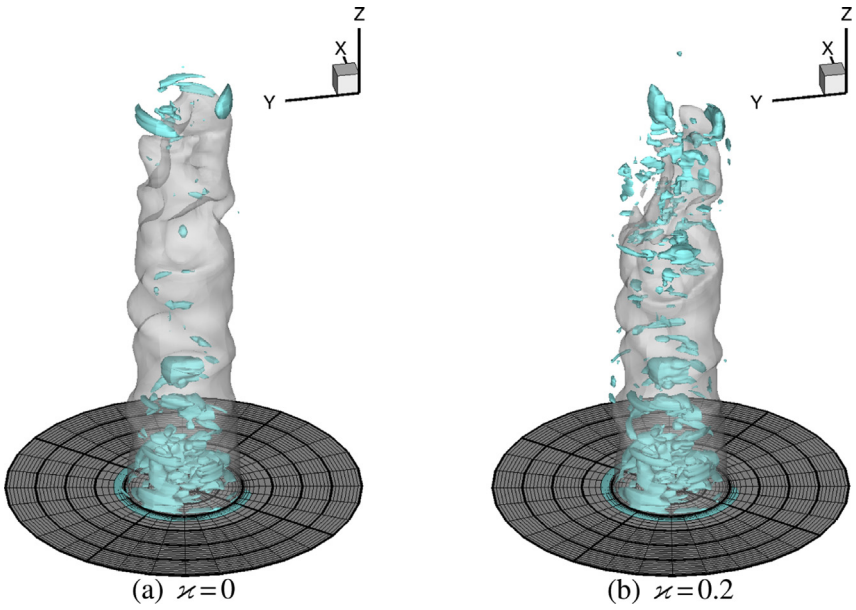

Fig. 6 – Instantaneous iso-surface $\tilde{T}=650$ K of the Bunsen-type flames (light grey) interacting with vortical structures (cyan) identified by $Q = 0.5(u'/L_t)^2 = 1606\ s^{-2}$ at 56 ms. Left: CH_4–air flame ($\varkappa=0$). Right: H_2–CH_4–air flame ($\varkappa=0.2$).

flame displays a higher degree of wrinkling with sharper ridges of negative curvature (curvature is negative in regions that are concave with respect to the unburned gas) and larger pockets of positive curvature, which are more pronounced near the flame tip. The vortical structures identified by the Q-criterion are similar in shape and number near the burner exit for both flames. Further downstream, the number of the coherent vortices decreases more rapidly for the pure methane–air flame, whereas a large number of turbulent structures is observed for the H_2-enriched flame, particularly in the highly wrinkled region near the flame tip. The addition of H_2 would seem to modify the interaction between the flame front and the turbulent field, which can be related to the less diffusive-thermally stable character of the H_2-enriched flame. It has been suggested that the diffusive-thermal instability could lead to self-turbulization of flames [58].

More details of the internal structure of the flames can be seen in Fig. 7, where planar cuts of the instantaneous mass fraction distributions of representative species are respectively shown. It is evident that the enriched flame is shorter, which can be ascribed to a faster consumption of the blended fuel. The enriched flame was found to have slightly higher flow temperatures, particularly in regions convex towards the combustible mixture of gases. In addition, more and sharper cusps that protrude the burned gas are observed in the enriched flame. Reduced levels of CO_2 (not shown) were also observed in the computed enriched flame. In contrast, the planar cuts of NO mass fractions of Fig. 7 display larger amounts of NO in the enriched flame. Areas of larger NO concentrations are localized downstream regions of positive curvature (convex towards the unburned gas) for the enriched case. These regions also coincide with areas of high temperature. The planar cuts of CO mass fractions show an intensified production of CO for the enriched flame in the highly wrinkled region near the flame tip, around the centerline. However, no significant difference of CO levels is noticeable in the fully burned gas zones of the two flames from these contours.

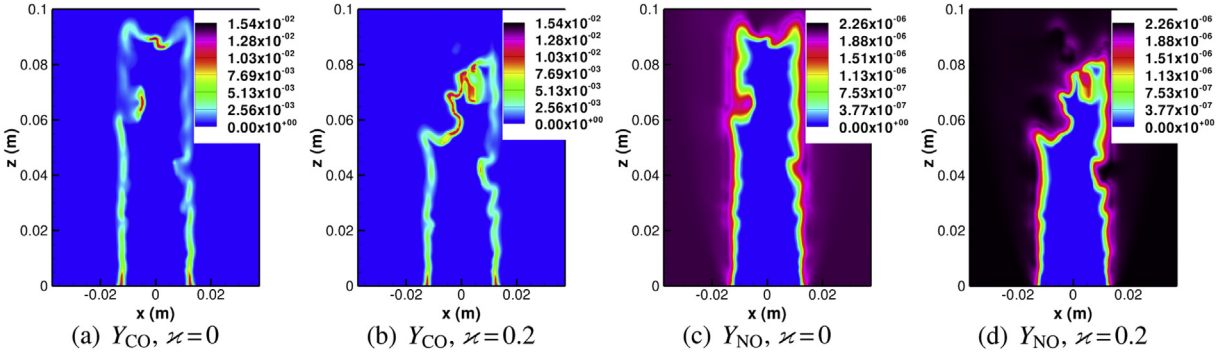

Fig. 7 – Planar cuts of the instantaneous CO and NO mass fraction distributions of the Bunsen-type flames at 56 ms. Plane y = 0. Left: CH_4–air flame ($\varkappa=0$). Right: H_2–CH_4–air flame ($\varkappa=0.2$).

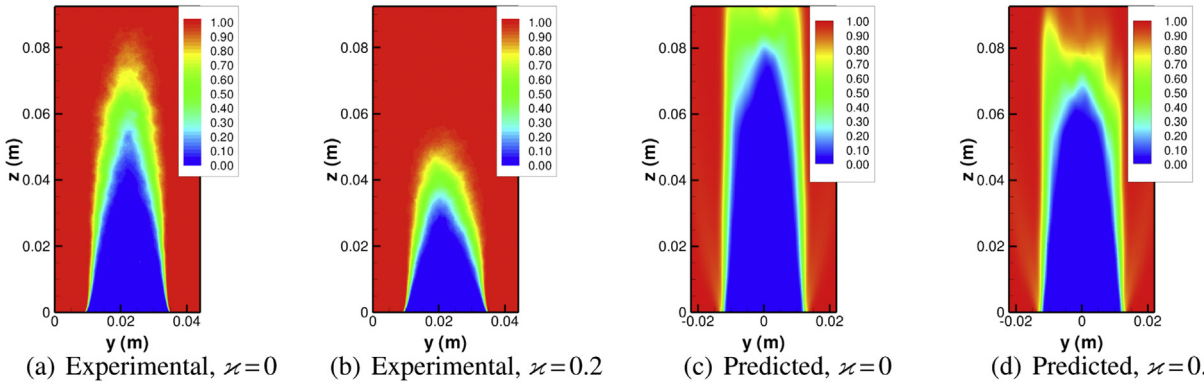

Fig. 8 – Comparison of experimental and predicted temperature-based flame brushes for the Bunsen-type CH_4–air ($\varkappa=0$) and H_2–CH_4–air ($\varkappa=0.2$) flames.

4.3. *Average flame structure*

To compare the numerical results with the experimental data of Halter et al. [22], a time-average of the LES solutions was performed over 70 ms (from 30 ms to 100 ms) using 71 instantaneous snapshots of each solution. Moreover, 2D slices of the resolved LES temperature field were extracted and processed to calculate progress variable fields based on temperature. The experimental flame brush was calculated using 500 Mie scattering images of oil droplets seeded in the fresh mixture of reactants [22]. The images were converted to a binary format and an edge-finding algorithm was applied to each instantaneous image to determine the progress variable maps. The resolution of the Mie scattering imaging procedure was 110 μm/pixel.

The experimental and numerical flame brushes are given in Fig. 8. Although clear differences between the experimental and numerical results can be seen, both the experiments and the simulations show a decrease in the flame height (36% and 18%, respectively, computed from the temperature-based progress variable $c_T = 0.1$ contour and evaluated at the centerline [22]) when hydrogen is added to methane, indicating a higher global burning rate for the enriched flame. It can also be observed that the predicted flames are taller than their experimental counterparts. It is worth noting that pockets of unburned gas were neglected (i.e., they were treated as burned gas) in the image analysis of Halter [22]. The presence of pockets of unburned gas near and above the flame tip in the instantaneous images would increase the height of the ensemble-averaged flame front. Therefore, the actual flame brushes are expected to be somewhat taller than those shown in Fig. 8.

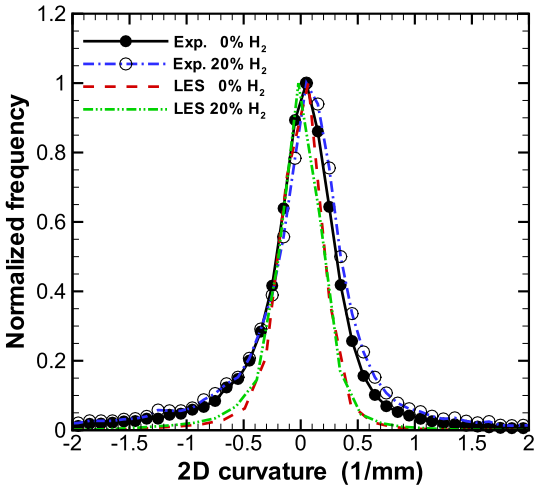

Fig. 9 – PDF of 2D curvature corresponding to a progress variable $c_T = 0.5$ for the Bunsen-type CH_4–air ($\varkappa=0$) and H_2–CH_4–air ($\varkappa=0.2$) flames.

Two-dimensional curvature was also extracted from instantaneous unfiltered experimental images and slices of the numerical solutions. The curvature PDFs from the experimental data and the LES solutions associated to the $c_T = 0.5$ contour are shown in Fig. 9. The PDFs display a Gaussian-type shape centred around zero, with the PDF corresponding to the predicted enriched flame being slightly skewed towards negative values of curvature. The PDFs corresponding to the LES simulations are narrower, owing to a smaller resolution of the flame front as compared to the experimental flame front images. It is apparent that the addition of hydrogen leads to slightly broader PDFs, in both the experiments and the simulations, with higher probabilities of finding larger curvatures for the enriched flame. This indicates that more small-scale wrinkling is present in the enriched flame.

5. Conclusions

In summary, the LES simulations of axisymmetric Bunsen-type turbulent premixed methane–air and H_2-enriched methane–air flames predicted similar qualitative trends to those found in the experiments of Halter et al. [22] for flame height and curvature. The enriched flame was shorter, which is attributed to a faster consumption of the blended fuel. The curvature PDFs displayed a Gaussian-type shape centred around zero. In both the experiments and the simulations, the addition of hydrogen lead to slightly broader PDFs. Furthermore, the hydrogen enriched flame displayed a higher degree of wrinkling with sharper ridges of negative curvature and

larger pockets of positive curvature, which were more pronounced near the flame tip. This behaviour has been associated with preferential diffusion effects and the less diffusive-thermally stable character of the H_2-enriched flame. In addition, reduced levels of CO_2 and increased levels of NO emissions were predicted for the enriched flame, and a slight increase in the CO levels in areas of fully burned gas was exhibited in the predicted enriched flame. All in all, the proposed treatment for the PCM-FPI combustion model, in terms of progress variable and tabulated data, appears to perform well for enriched methane flames in the methane-dominated regime. Further study is warranted for a wider class of flames.

Acknowledgements

Financial support for the research described herein was provided by the MITACS (Mathematics of Information Technology and Complex Systems) Network, part of the Networks of Centres of Excellence (NCE) program funded by the Canadian Government. This funding is gratefully acknowledged with many thanks. The first author gratefully acknowledges the financial support from the Mexican National Council for Science and Technology (CONACyT). The authors are also grateful to Dr. Fabien Halter for providing the experimental data used in the comparisons with the predicted LES solutions. Computational resources for performing all of the calculations reported herein were provided by the SciNet High Performance Computing Consortium at the University of Toronto and Compute/Calcul Canada through funding from the Canada Foundation for Innovation (CFI) and the Province of Ontario, Canada.

REFERENCES

[1] Edwards PP, Kuznetsov VL, David WIF. Hydrogen energy. Phil Trans R Soc A 2007;365:1043–56.
[2] Muradov NZ, Veziroğlu TN. "Green" path from fossil-based to hydrogen economy: an overview of carbon-neutral technologies. Int J Hydrogen Energy 2008;33:6804–39.
[3] Budzianowski WM. An oxy-fuel mass-recirculating process for H_2 production with CO_2 capture by autothermal catalytic oxyforming of methane. Int J Hydrogen Energy 2010;35:7454–69.
[4] Nagalingam B, Duebel F, Schmillen K. Performance study using natural gas, hydrogen-supplemented natural gas and hydrogen in AVL research engine. Int J Hydrogen Energy 1983;8:715–20.
[5] Bell SR, Gupta M. Extension of the lean operating limit for natural gas fueling of spark ignited engine using hydrogen blending. Combust Sci Tech 1997;123:23–48.
[6] Bauer CG, Forest T. Effect of hydrogen addition on the performance of methane-fueled vehicles. Part I: effect on S.I. engine performance. Int J Hydrogen Energy 2001;26:71–7.
[7] Kumar MS, Ramesh A, Nagalingam B. Use of hydrogen to enhance the performance of a vegetable oil fuelled compression ignition engine. Int J Hydrogen Energy 2003;28:1143–54.
[8] Yu G, Law CK, Wu CK. Laminar flame speeds of hydrocarbon + air mixtures with hydrogen addition. Combust Flame 1986;63:339–47.
[9] Gauducheau JL, Denet B, Searby G. A numerical study of lean CH_4/H_2 premixed flames at high pressure. Combust Sci Tech 1998;137:81–99.
[10] Ren J-Y, Qin W, Egolfopoulos FN, Tsotsis TT. Strain-rate effects on hydrogen-enhanced lean premixed combustion. Combust Flame 2001;124:717–20.
[11] Jackson GS, Sai R, Plaia JM, Boggs CM, Kiger KT. Influence of H_2 on the response of lean premixed CH_4 flames to high strained flows. Combust Flame 2003;132:503–11.
[12] Guo H, Smallwood GJ, Liu F, Ju Y, Gülder OL. The effect of hydrogen addition on flammability limit and NO_x emission in ultra-lean counterflow CH_4/air premixed flames. Proc Combust Inst 2005;30:303–11.
[13] Schefer RW. Hydrogen enrichment for improved lean flame stability. Int J Hydrogen Energy 2003;28:1131–41.
[14] Kim HS, Arghode VK, Gupta AK. Flame characteristics of hydrogen-enriched methane-air premixed swirling flames. Int J Hydrogen Energy 2009;34:1063–73.
[15] di Sarli V, di Benedetto A. Laminar burning velocity of hydrogen–methane/air premixed flames. Int J Hydrogen Energy 2007;32:637–46.
[16] Hawkes ER, Chen JH. Direct numerical simulation of hydrogen-enriched lean premixed methane-air flames. Combust Flame 2004;138:405–36.
[17] Dunstan TD, Jenkins KW. The efects of hydrogen substitution on turbulent premixed methane-air kernels using direct numerical simulation. Int J Hydrogen Energy 2009;34:8389–404.
[18] Day MS, Gao X, Bell JB. Properties of lean turbulent methane-air flames with significant hydrogen addition. Proc Combust Inst 2011;33:1601–8.
[19] Vreman AW, van Oijen JA, de Goey LPH, Bastiaans RJM. Direct numerical simulation of hydrogen addition in turbulent premixed bunsen flames using flamelet-generated manifold reduction. Int J Hydrogen Energy 2009;34:2778–88.
[20] Domingo P, Vervisch L, Payet S, Hauguel R. DNS of a premixed turbulent V flame and LES of a ducted flame using a FSD-PDF subgrid scale closure with FPI-tabulated chemistry. Combust Flame 2005;143:566–86.
[21] Gicquel O, Darabiha N, Thévenin D. Laminar premixed hydrogen/air counterflow flame simulations using flame prolongation of ILDM with differential diffusion. Proc Combust Inst 2000;28:1901–8.
[22] Halter F, Chauveau C, Gökalp I. Characterization of the effects of hydrogen addition in premixed methane/air flames. Int J Hydrogen Energy 2007;32:2585–92.
[23] Hernández-Pérez FE. Subfilter scale modelling for large eddy simulation of lean hydrogen-enriched turbulent premixed combustion. University of Toronto; April 2011 [Ph.D. thesis].
[24] Hernández-Pérez FE, Yuen FTC, Groth CPT, Gülder OL. LES of a laboratory-scale turbulent premixed bunsen flame using FSD, PCM-FPI and thickened flame models. Proc Combust Inst 2011;33:1365–71.
[25] Yoshizawa A. Statistical theory for compressible turbulent shear flows with the application to subgrid modeling. Phys Fluids A 1986;29:2152–64.
[26] Knight D, Zhou G, Okong'o N, Shukla V. Compressible large eddy simulation using unstructured grids. AIAA; January 1998. Paper 98–0535.
[27] van Oijen JA, de Goey LPH. Modelling of premixed laminar flames using flamelet-generated manifolds. Combust Sci Tech 2000;161:113–37.
[28] van Oijen JA, Lammers FA, de Goey LPH. Modeling of complex premixed burner systems by using flamelet-generated manifolds. Combust Flame 2001;127(3):2124–34.
[29] van Oijen JA, de Goey LPH. Modelling of premixed counterflow flames using the flamelet-generated manifold method, Combust. Theory Model 2002;6(3):463–78.

[30] Domingo P, Vervisch L, Veynante D. Large-eddy simulation of a lifted methane jet flame in a vitiated coflow. Combust Flame 2008;152:415–32.
[31] Galpin J, Naudin A, Vervisch L, Angelberger C, Colin O, Domingo P. Large-eddy simulation of a fuel-lean premixed turbulent swirl-burner. Combust Flame 2008;155:247–66.
[32] Bray KNC, Champion M, Libby PA, Swaminathan N. Finite rate chemistry and presumed PDF models for premixed turbulent combustion. Combust Flame 2006;146:665–73.
[33] Jin B, Grout R, Bushe WK. Conditional source-term estimation as a method for chemical closure in premixed turbulent reacting flow. Flow Turb Combust 2008;81:563–82.
[34] Salehi MM, Shahabazian N, Bushe WK, Groth CPT, Gauthier PQ. Presumed PDF modelling for LES of turbulent premixed combustion. In: Proceedings of the combustion institute/Canadian section spring technical meeting, Toronto, Ontario, Canada, May 13–16, 2012. Combustion Institute/Canadian Section; 2012. pp. 320–5.
[35] Salehi MM, Bushe WK, Shahbazian N, Groth CPT. Modified laminar flamelet presumed probability density function for LES of premixed turbulent combustion. Proc Combust Inst 2013;34:1203–11.
[36] Shahbazian N, Groth CPT, Gülder OL. Assessment of presumed PDF models for large eddy simulation of turbulent premixed flames. Paper 2011-0781. AIAA; January 2011.
[37] Gao X, Groth CPT. A parallel adaptive mesh refinement algorithm for predicting turbulent non-premixed combusting flows. Int J Comput Fluid Dyn 2006;20(5):349–57.
[38] Gao X, Groth CPT. Parallel adaptive mesh refinement scheme for three-dimensional turbulent non-premixed combustion. Paper 2008-1017. AIAA; January 2008.
[39] Gao X, Groth CPT. A parallel solution-adaptive method for three-dimensional turbulent non-premixed combusting flows. J Comput Phys 2010;229(5):3250–75.
[40] Gao X, Northrup SA, Groth CPT. Parallel solution-adaptive method for two-dimensional non-premixed combusting flows. Prog Comput Fluid Dyn 2011;11(2):76–95.
[41] Lin W, Hernández-Pérez FE, Groth CPT, Gülder OL. Comparison of subfilter scale models for LES of turbulent premixed flames. Paper 2008-1048. AIAA; January 2008.
[42] Lin W. Large-eddy simulation of premixed turbulent combustion using flame surface density approach [Ph.D. thesis]. University of Toronto; August 2010.
[43] Barth TJ. Recent developments in high order k-exact reconstruction on unstructured meshes. Paper 93–0668. AIAA; January 1993.
[44] Roe PL. Approximate Riemann solvers, parameter vectors, and difference schemes. J Comput Phys 1981;43:357–72.
[45] Liou M-S. A sequel to AUSM, part ii: AUSM$^+$-up for all apeeds. J Comput Phys 2006;214:137–70.
[46] Mathur SR, Murthy JY. A pressure-based method for unstructured meshes. Numer Heat Trans 1997;31:191–215.
[47] Gropp W, Lusk E, Skjellum A. Using MPI. Cambridge, Massachussets: MIT Press; 1999.
[48] Gropp W, Lusk E, Thakur R. Using MPI-2. Cambridge, Massachussets: MIT Press; 1999.
[49] Fiorina B, Gicquel O, Vervisch L, Carpentier S, Darabiha N. Premixed turbulent combustion modeling using tabulated detailed chemistry and PDF. Proc Combust Inst 2005;30:867–74.
[50] California Institute of Technology. CANTERA release 1.7 http://code.google.com/p/cantera; 2006.
[51] Smith GP, Golden DM, Frenklach M, Moriarty NW, Eiteneer B, Goldenberg M, et al. GRI-mech 3.0 http://www.me.berkeley.edu/gri_mech/; 2000.
[52] Ren J-Y, Qin W, Egolfopoulos FN, Mak H, Tsotsis TT. Methane reforming and its potential effect on the efficiency and pollutant emissions of lean methane–air combustion. Chem Eng Sci 2001;56:1541–9.
[53] Bradley D, Gaskell PH, Gu XJ, Lawes M, Scott MJ. Premixed turbulent flame instability and NO formation in a lean-burn swirl burner. Combust Flame 1998;115:515–38.
[54] Godel G, Domingo P, Vervisch L. Tabulation of NO_x chemistry for large-eddy simulation of non-premixed turbulent flames. Proc Combust Inst 2009;32:1555–61.
[55] Hill SC, Smoot LD. Modeling of nitrogen oxides formation and destruction in combustion systems. Prog Energy Combust Sci 2000;26:417–58.
[56] Frassoldati A, Frigerio S, Colombo E, Inzoli F, Faravelli T. Determination of NO_x emissions from strong swirling confined flames with an integrated CFD-based procedure. Chem Eng Sci 2005;60:2851–69.
[57] Hunt JCR, Wray AA, Moin P. Eddies, stream, and convergence zones in turbulent flows, annual research brief. Center for Turbulence Research, Stanford University; 1988.
[58] Sivashinsky GI. Instabilities, pattern formation, and turbulence in flames. Ann Rev Fluid Mech 1983;15:179–99.